Magnetic Resonance in Medicine 64:1607–1615 (2010)

Intracellular and Extracellular T_1 and T_2 Relaxivities of Magneto-Optical Nanoparticles at Experimental High Fields

Gert Klug,[1*†] Thomas Kampf,[2] Steffen Bloemer,[3] Johannes Bremicker,[1] Christian H. Ziener,[2] Andrea Heymer,[4] Uwe Gbureck,[5] Eberhard Rommel,[2] Ulrich Nöth,[4] Wolfdieter A. Schenk,[3] Peter M. Jakob,[2] and Wolfgang R. Bauer[1]

This study reports the T_1 and T_2 relaxation rates of rhodamine-labeled anionic magnetic nanoparticles determined at 7, 11.7, and 17.6 T both in solution and after cellular internalization. Therefore cells were incubated with rhodamine-labeled anionic magnetic nanoparticles and were prepared at decreasing concentrations. Additionally, rhodamine-labeled anionic magnetic nanoparticles in solution were used for extracellular measurements. T_1 and T_2 were determined at 7, 11.7, and 17.6 T. T_1 times were determined with an inversion-recovery snapshot-flash sequence. T_2 times were obtained from a multispin-echo sequence. Inductively coupled plasma-mass spectrometry was used to determine the iron content in all samples, and r_1 and r_2 were subsequently calculated. The results were then compared with cells labeled with AMI-25 and VSOP C-200. In solution, the r_1 and r_2 of rhodamine-labeled anionic magnetic nanoparticles were 4.78/379 (7 T), 3.28/389 (11.7 T), and 2.00/354 (17.6 T). In cells, the r_1 and r_2 were 0.21/56 (7 T), 0.19/37 (11.7 T), and 0.1/23 (17.6 T). This corresponded to an 11- to 23-fold decrease in r_1 and an 8- to 15-fold decrease in r_2. A decrease in r_1 was observed for AMI-25 and VSOP C-200. AMI-25 and VSOP exhibited a 2- to 8-fold decrease in r_2. In conclusion, cellular internalization of iron oxide nanoparticles strongly decreased their T_1 and T_2 potency. Magn Reson Med 64:1607–1615, 2010. © 2010 Wiley-Liss, Inc.

Key words: iron oxide nanoparticles; relaxivities; cellular internalization; high field

The unique soft-tissue contrast achieved by magnetic resonance imaging (MRI) originates from the variations of longitudinal (T_1) and transversal (T_2/T_2*) proton relaxation rates between different tissues. T_1- and T_2-shortening contrast agents are commonly used to enhance contrast. T_1-shortening results in enhanced signal and/or faster imaging due to a higher value of available longitudinal magnetization for repetitive excitations. Because of faster spin relaxation, T_2-shortening results in less signal but even higher contrast. As all contrast agents lower T_1 and T_2, the ratio of the molar relaxivities (r_1/r_2) is commonly used to describe their features.

Superparamagnetic iron oxides particles (SPIOs) mainly shorten T_2/T_2* (r_1/r_2 at 0.47 T: 0.2–0.6) (1–3); therefore, they are considered as "negative contrast" agents. For high field strengths above 2 T, r_1 decreases to zero and r_2 approaches a constant nonzero value. This results in a significant shift of the r_1/r_2 ratio to lower values (r_1/r_2 at 7 T: 0.01–0.1) (3–6). Therefore, at field strengths above 7 T, T_2/T_2*-weighted imaging sequences are commonly used for SPIO-enhanced MRI. In contrast to "positive" extracellular Gadolinium (Gd) chelates (r_1/r_2 of Gd-DTPA at 0.47 T: >0.6), SPIOs remain in the healthy vasculature and are internalized by reticuloendothelial system cells after intravenous injection. Depending on their physicochemical properties, they are applied to MR-angiography, liver imaging (Kupffer cells), and molecular imaging (6,7). Recently, the synthesis of a novel rhodamine-labeled anionic magnetic nanoparticle (Rh-AMNP) was described by Bertorelle et al. (8). AMNPs exhibit favorable cellular uptake and T_2 relaxation rates (r_1: 11.7 mM^{-1} s^{-1} and r_2: 363 mM^{-1} s^{-1} at 1.5 T) (9). In combination with an attached fluorescent dye, these characteristics make them good candidates for experimental cell-tracking studies.

Experimental studies on various SPIOs have been performed to characterize the effects of cellular internalization on R_1 and R_2 at field strengths ranging from 1.5 to 7 T (4,9,10). It has been reported that both the r_1 and r_2 of iron oxide nanoparticles are reduced by cellular internalization. The reduction of r_1 by cellular internalization can be explained by an exchange model. In this model, two different pools of protons exist: a small intracellular pool with high r_1, due to the internalized contrast agent, and a large extracellular pool with low r_1. Because of restricted diffusion, the exchange of water protons between both pools is limited and thus the apparent r_1 relaxivity of intracellular iron oxides decreases when compared with freely dispersed contrast agents. The decrease in r_2 is attributable to the fact that internalized iron oxide particles form larger "quasiparticles." Furthermore, the conditions of the motional narrowing regime are no longer fulfilled (11). Thus, the refocusing of spins using

[1]Medizinische Klinik und Poliklinik I, Universitätsklinik Würzburg, Würzburg, Germany.
[2]Experimentelle Physik 5, Universität Würzburg, Würzburg, Germany.
[3]Institut für Anorganische Chemie, Universität Würzburg, Würzburg, Germany.
[4]Division of Tissue Engineering, König-Ludwig-Haus, Würzburg, Germany.
[5]Department of Functional Materials in Medicine and Dentistry, Universität Würzburg, Würzburg, Germany.
[†]*Present address:* Universitätsklinik für Innere Medizin III, Medizinische Universität Innsbruck, Austria.
Grant sponsor: Deutsche Forschungsgemeinschaft; Grant number: DFG-SFB 688; Grant sponsor: Berufsverband Deutscher Internisten.
*Correspondence to: Gert Klug, MD, Universitätsklinik für Innere Medizin III, Medizinsche Universität Innsbruck, Austria. E-mail: Gert.Klug@uki.at
Received 30 April 2009; revised 26 May 2010; accepted 16 June 2010.
DOI 10.1002/mrm.22557
Published online 27 July 2010 in Wiley Online Library (wileyonlinelibrary.com).

spin-echo experiments is more efficient, leading to a lower r_2 relaxivity.

In general, despite the growing importance of high magnetic fields in MRI, there is little experimental data on the relaxivities of SPIOs at ultrahigh field (>7 T) (4). As it is important to extend recent results on the change of relaxation effects after intracellular compartmentalization, this study aimed to (a) provide data on the molar relaxivities of Rh-AMNP at 7 T, 11.7 T, and 17.6 T; (b) quantify the effect of cellular internalization on the molar relaxivities at these field strengths; and (c) compare the obtained results to commercially available SPIOs.

MATERIALS AND METHODS

Contrast Agent

Anionic magnetite nanoparticles coated with *meso*-2,3-dimercaptosuccinic acid and labeled with dimethylrhodamine (Rh-AMNP) were synthesized through high-temperature solution phase reaction of iron (III) acetylacetonate. This was done in the presence of 1,2-decanediol, oleic acid, and oleylamine (12). The hydrophobic capping of the particles was stripped with a solution of ammonia in *n*-butanol (13), and the naked particles were resuspended in aqueous *meso*-2,3-dimercaptosuccinic acid at pH = 7.3. The subsequent water-soluble iron oxide particles were finally coupled with the fluorescent dye tetramethylrhodamine-5-maleimide (Molecular Probes, Invitrogen, Eugene, OR).

Sample Preparation

Rh-AMNP was homogeneously suspended in Ficoll solution (Amersham Bioscience, GE Healthcare, Uppsala, Sweden) for relaxometry of free undispersed contrast media at concentrations ranging from 40 to 5 μg Fe mL^{-1}. Ficoll solution without any contrast agent served as the reference standard in these experiments.

Immortalized peritoneal mouse macrophages obtained from the continuously growing murine macrophage cell line PMJ2-R (ATCC [CRL-2458], Manassas, VA) were used for cell-labeling studies. Cells were grown in Dulbecco's modified Eagle's medium with 4 mM L-glutamine adjusted to contain 1.5 g L^{-1} sodium bicarbonate and 4.5 g L^{-1} glucose. This was then supplemented with 5 mM of 4-(2-hydroxyethyl)-1-piperazineethanesulfonic acid (HEPES), 95%, and fetal bovine serum, 5%.

Cells (1×10^8) were incubated with Rh-AMNP at a concentration of 100 μg Fe mL^{-1} in 30 mL medium for 4 h and afterward washed three times. Within 1 h thereafter, the medium containing the labeled, living cells was increasingly diluted with Ficoll solution (pH 7.5) to obtain the following concentrations: 2.5×10^7, 1.25×10^7, 6.25×10^6, and 3.12×10^6 cells/0.5 mL. Unlabeled cells (2.5×10^7) served as the reference standard. Assuming a mean cell diameter of $d = 8$ μm (14), the volume fraction of cells within the phantoms ranged from 0.17% (3.12×10^6 cells/0.5 mL) to 1.32% (2.5×10^7 cells/0.5 mL).

The same experimental setup was used to compare the cellular uptake of Rh-AMNP with Ferumoxide (AMI-25, Endorem®, Guerbet, France) and VSOP-C200 (Ferropharm, Teltow, Germany). Each cell-labeling protocol was performed in duplicate or triplicate.

MR Relaxometry and Data Analysis

Relaxometry was performed on a 7 T BIOSPEC (proton frequency: 300 MHz), an 11.7 T AMX (500 MHz), and a 17.6 T AVANCE (750 MHz) scanner (all Bruker BioSpin GmbH, Rheinstetten, Germany). Global scan setup contained manual tuning and matching as well as quadratic shimming. Additionally, the gradient-system cooling/heating was set to 19–21°C to ensure a constant temperature of 20 °C for all samples in all scanners.

Before and after measurements, multislice gradient-echo scout images were axially acquired from all five cell phantoms to ensure homogeneous distribution of the solution and cells (TE: 6 ms). T_1 measurements were performed with an inversion-recovery snapshot fast low-angle shot (IRSFL) sequence (FA_{FLASH}: 8°, TR_{FLASH}: 3.29 ms, TE_{FLASH}: 1.645 ms, 100 frames, voxel size: 0.625 mm × 0.625 mm × 4 mm). T_2 measurements were performed using a multispin-echo sequence consisting of a Carr-Purcell-Meiboom-Gill (CPMG) train (FA: 90°/180°; pulse repetition time [TR]: 5000 ms; TE/inter echo time: 6 ms, 250 echoes; voxel size: 0.625 mm × 0.625 mm × 4 mm).

Data were quantitatively analyzed off-line with the use of home-written MATLAB routines (The MathWorks, Natick, MA). T_1 and T_2 maps were generated assuming monoexponential relaxation and using a nonlinear least-square fit with the following equations:

$$\mathrm{SI}(t) = A - Be^{(-t/T_1^*)} \quad [1]$$

with

$$T_1 = (B/A - 1)T_1^* \quad [2]$$

for longitudinal relaxation (15) and

$$\mathrm{SI}(t) = SI_0 e^{(-t/T_2)} + B \quad [3]$$

for transverse relaxation.

Comparison with AMI-25 and Citrate-Coated SPIOs

To compare the results obtained with Rh-AMNP to commercially available SPIOs, AMI-25 and VSOP-C200 were chosen. AMI-25 consists of a Fe_2O_3/Fe_3O_4 core (diameter: 4–5 nm) with a neutral dextran T10 coating. It is manufactured as beads with a hydrodynamic diameter of 120–180 nm. In contrast, the Fe_2O_3/Fe_3O_4 core of VSOP-C200 (diameter: 5 nm) is coated by monomeric citrate, resulting in a total hydrodynamic diameter of ~10 nm and an anionic surface charge.

The same experimental setup was used to compare the cellular uptake of Rh-AMNP with AMI-25 and VSOP-C200. After preparing the samples analogous to the Rh-AMNP phantoms, r_1 and r_2 were determined at 7 T, 11.7 T, and 17.6 T, as previously described.

Histology and Inductively Coupled Mass Spectrometry

After labeling, the percentage of nonviable cells was determined via a Trypan blue exclusion test. After MR

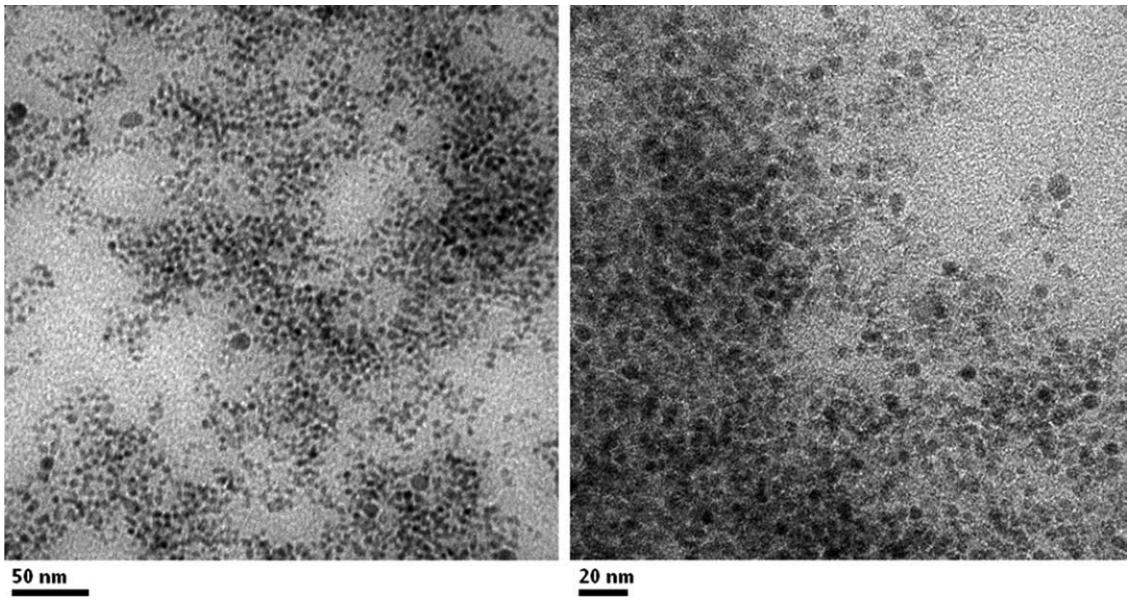

FIG. 1. Transmission electron microscopy images show iron oxide cores of 4–5 nm. The coating material separates the particles but is not visualized because of the lack of electron density of *meso*-2,3-dimercaptosuccinic acid for detection with TEM. The particles are well separated and do not aggregate.

sessions, Prussian blue staining was performed and fluorescent images were obtained using a Rhodamine filter (absorption/emission = 540/567 nm). Fluorescent images were then merged offline with bright-field images. Iron content in the cells and solution were determined by inductively coupled plasma-mass spectrometry (ICP-MS). For ICP-MS, samples were mixed to 1:1 with 65% HNO_3 for at least 12 h and then diluted to 1:9 with ultrapure H_2O.

Statistical Analysis

The relaxation rates R_1 and R_2 were calculated from measured T_1 and T_2 values through

$$R_x = \frac{1}{T_x}, \qquad [4]$$

where x is either 1 or 2. The changes in R_1 and R_2 for each sample compared with the reference standard were then plotted against the iron concentration with SPSS 16.0.1 for Windows (SPPS, Chicago, IL). Molar relaxivities r_1 and r_2 (mM^{-1} s^{-1}) were deduced from the linear fit forced through $(x,y) = (0,0)$. The quality of the least-square fit through the data points was given by r, and data were presented as mean ± standard deviation.

RESULTS

Rh-AMNP Synthesis

Transmission electron microscopy of synthesized Rh-AMNP particles revealed a mean iron core diameter of 4–5 nm. Because of the low electron density, the coating layer of Rh-labeled *meso*-2,3-dimercaptosuccinic acid could not be observed on transmission electron microscopy images. However, the particles were monodisperse, well separated, and did not aggregate (Fig. 1).

Rh-AMNP Cellular Uptake

According to the Trypan blue exclusion test, >90% of the cells were labeled viable, which was in the range of unlabeled cells and AMI-25- or VSOP C-200-labeled cells. Rhodamine fluorescence signal was colocalized with Prussian Blue staining (Fig. 2). Based on the assumption of homogeneous iron content throughout all cells, iron per cell was calculated for each sample after iron quantification with ICP-MS. Iron per cell ranged

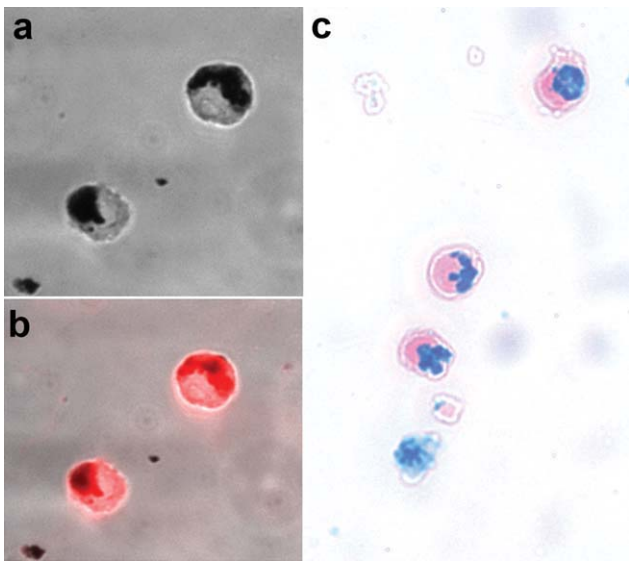

FIG. 2. Cells of a murine macrophage cell line labeled with Rh-AMNP. Fluorescent and bright-field microscopy reveals the colocalization of iron (**a**, dark) and rhodamine fluorescent signal (**b**, red). Prussian blue histology of the cells confirms intracellular uptake of iron (**c**, blue). [Color figure can be viewed in the online issue, which is available at wileyonlinelibrary.com.]

Table 1
Comparison of Different Iron Oxide Contrast Agents with Respect to Their Cellular Uptake

Contrast agent	Cell number (10^6/0.5 mL)	Iron/sample		Iron/cell (pg per cell)
		ICPMS (ppb)	Sample (0.5 ml) (μg/mL)	
Rh-AMNP	25	949 ± 10	18.9 ± 0.2	0.38 ± 0.004
	12.5	711 ± 47	14.2 ± 0.9	0.57 ± 0.04
	6.25	316 ± 80	6.3 ± 1.6	0.50 ± 0.13
	3.12	194 ± 22	3.9 ± 0.4	0.62 ± 0.07
	Mean			*0.51 ± 0.11*
AMI-25	25	399 ± 40	8.0 ± 0.8	0.16 ± 0.02
	12.5	200 ± 7	4.0 ± 0.1	0.16 ± 0.01
	6.25	107 ± 12	2.1 ± 0.2	0.17 ± 0.02
	3.12	48.8 ± 4.2	1.0 ± 0.1	0.16 ± 0.01
	Mean			*0.16 ± 0.01*
VSOP C-200	25	3092 ± 564	61.8 ± 11.2	1.24 ± 0.23
	12.5	1602 ± 510	32.1 ± 10.2	1.28 ± 0.41
	6.25	841 ± 278	16.8 ± 5.6	1.35 ± 0.45
	3.12	460 ± 225	9.20 ± 4.5	1.47 ± 0.72
	Mean			*1.33 ± 0.44*
Controls	25	11 ± 19	0.2 ± 0.4	0.005 ± 0.008

Because of sample preparation, the dilution factor of the ICP-MS samples was 20.

from 0.38 to 0.67 pg per cell with high reproducibility (Table 1).

Relaxivities of Suspended Iron Oxides

Signal intensities showed a monoexponential behavior for all samples over time (Figs. 3 and 4). The mean T_1 and T_2 relaxation times of the prepared phantoms correlated with the iron concentration measured by ICP-MS (Fig. 5). The samples with the highest iron concentrations (40 μg mL^{-1}) showed T_2 times lower than the shortest TE of 6 ms and were not included in further analysis. Furthermore, the change in the relaxation rates

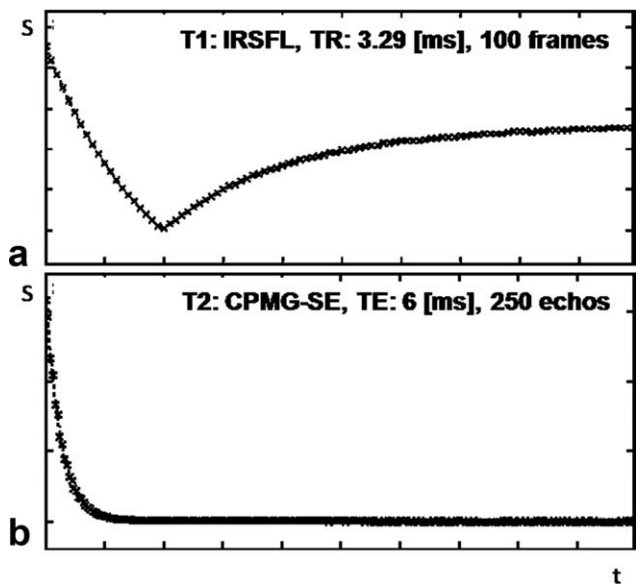

FIG. 3. Examples of T_1 (**a**) and T_2 (**b**) signal-to-time curves obtained by IRSFL and CPMG-SE sequences plotted with MATLAB. The magnitude of the signal (*S*) is plotted against the time (*t*), and the curves are fitted with monoexponential fits to obtain T_1 (ms) and T_2 (ms) (cf. Fig. 4).

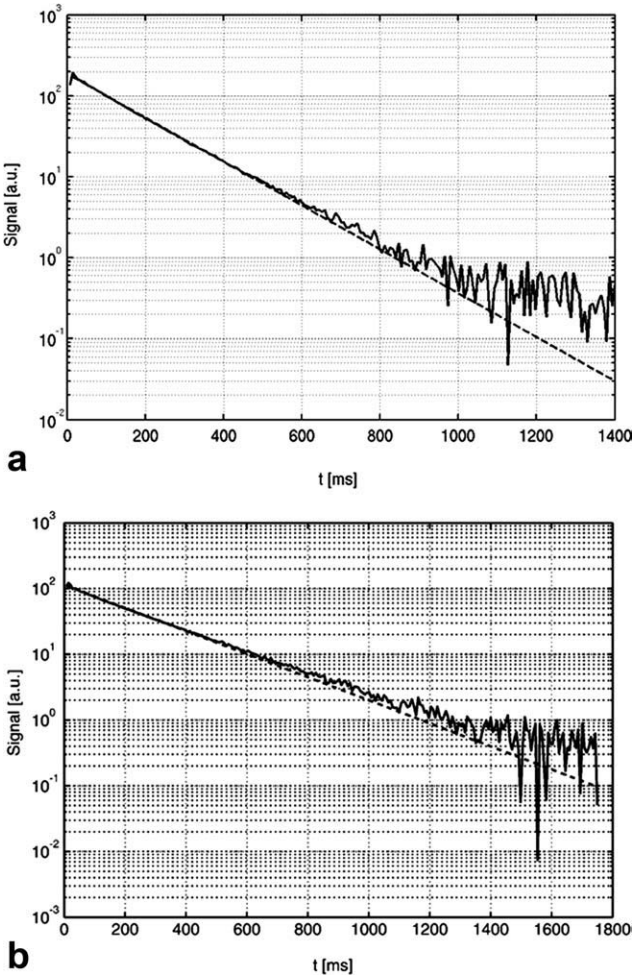

FIG. 4. Semilog plots of T_2 decays proving strictly monoexponential behavior. These were obtained by CPMG-SE sequences from samples with freely dispersed (**a**) and internalized contrast agents (**b**).

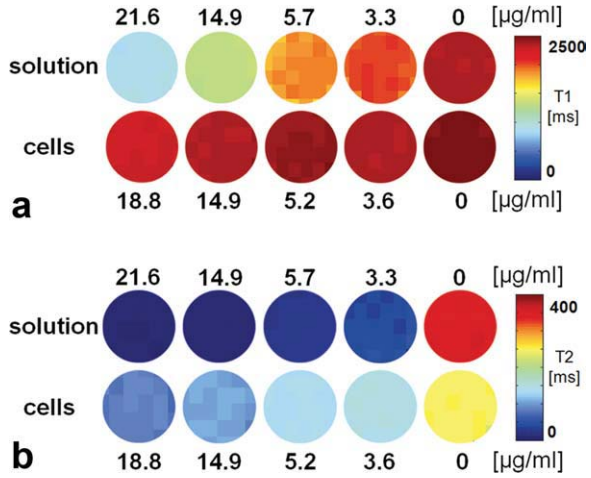

FIG. 5. Representative T_1 (**a**) and T_2 (**b**) maps obtained from samples with decreasing concentrations of Rh-AMNPs at 17.6 T. Although the iron concentrations in cell samples are similar to those of freely dispersed contrast agent, a marked reduction in the r_1 and r_2 is obvious.

R_1 and R_2 was linearly correlated to the iron concentration of the samples (all: $r > 0.97$; $P < 0.05$; Fig. 6). The longitudinal molar relaxivity, r_1, of Rh-AMNPs decreased with the applied field strength (r_1: 4.78 [7 T]; 3.28 [11.7 T]; and 2.00 [17.6 T] [mM^{-1} s^{-1}]; Table 2). The transverse relaxivity r_2, showed a plateau between 7 T and 17.6 T (r_2: 379 [7 T]; 386 [11.7 T]; and 354 [17.6 T] [mM^{-1} s^{-1}]; Table 2) (Fig. 7). The ratio r_1/r_2 therefore decreased as field strengths were increased (Table 2).

Relaxivities of Intracellular Iron Oxides

T_1 showed no significant differences for either the unlabeled cells or the pure Ficoll solution and ranged from 2171 to 2474 ms at different field strengths. T_2 times, however, were decreased in the presence of unlabeled cells (Ficoll vs. cells: 256/235 ms [7 T]; 328/219 ms [11.7 T]; and 349/248 ms [17.6 T]; Fig. 5). After cellular internalization, the T_1 and T_2 values of corresponding iron concentrations were significantly prolonged when compared with freely suspended particles (Fig. 5). Within the evaluated cell density range (5×10^7 per mL^{-1} to 6.2×10^6 per mL^{-1}) and iron concentrations (3.6 to 19.1 µg mL^{-1}), only monoexponential signal decays were observed for T_2 decays (Fig. 4). Using gradient echo scouts, no signal inhomogeneities due to cell clustering were observed in the samples within 30 min. Therefore, all samples were included in further analysis.

The change in relaxation rates showed excellent correlation with the iron concentration (all: $r > 0.95$; $P < 0.05$; Fig. 5). When compared with free iron oxides, the

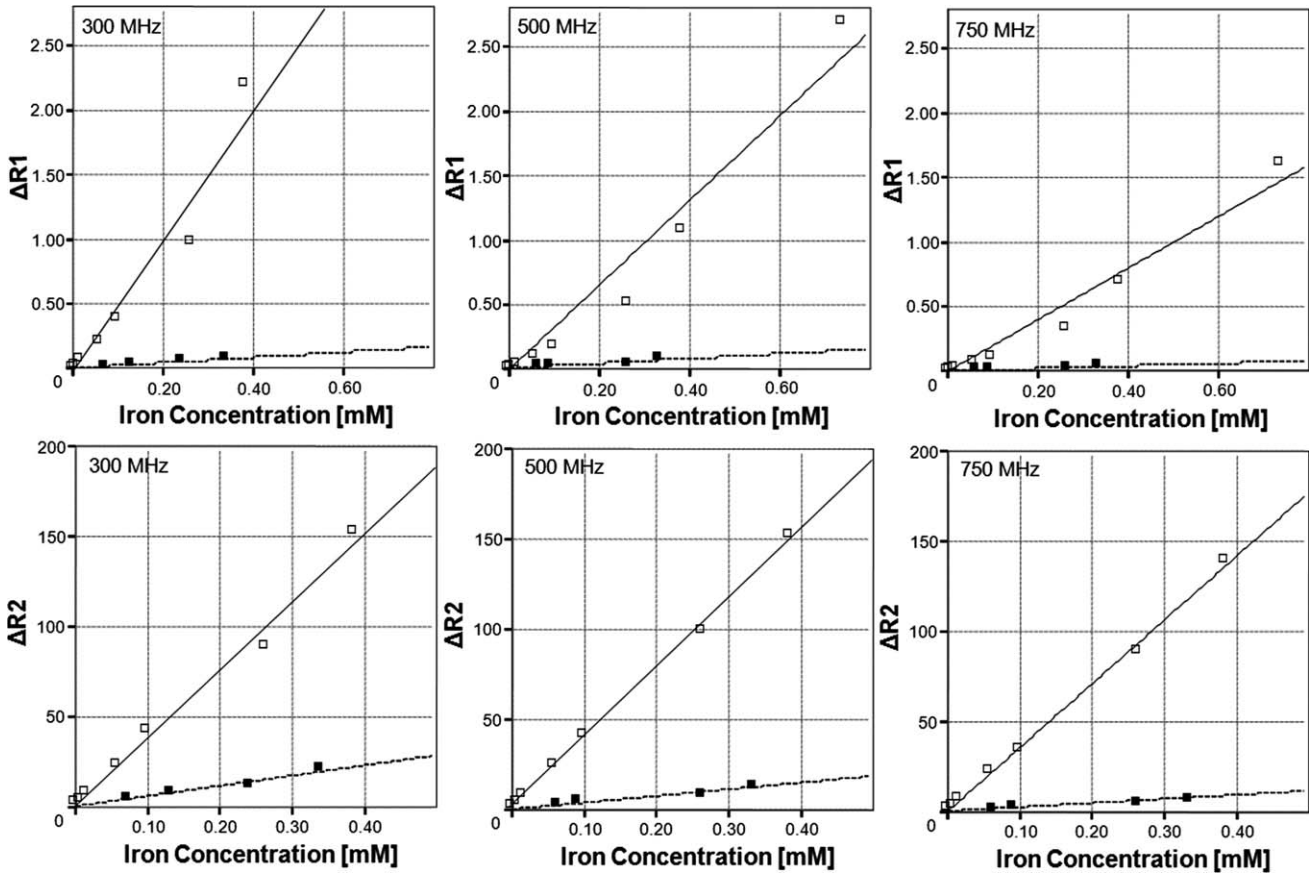

FIG. 6. Scatter plots showing the changes in relaxation rates as a function of the iron concentration at 7 T (300 MHz), 11.6 T (500 MHz), and 17.6 T (750 MHz). Open boxes show the values obtained for free Rh-AMNPs, and solid boxes display the values obtained from cell samples. Lines represent the least-squares fit through the data points and were forced through $(x,y) = (0,0)$.

Table 2
The r_1 and r_2 Values of Rh-AMNP, AMI-25, and VSOPs

Contrast agent	Proton frequency (MHz)	r_1				r_2				r_1/r_2	
		In solution		In cells		In solution		In cells			
		(mM^{-1} s^{-1})	r	(s^{-1} mM^{-1})	r	(s^{-1} mM^{-1})	r	(s^{-1} mM^{-1})	r	In solution	In cells
AMNP (9)	63	10.2	–	1.1	–	357	–	248	–	0.029	0.004
Rh-AMNP	300	4.78	>0.97	0.21	>0.99	379	>0.99	56	>0.99	0.012	0.004
Rh-AMNP	500	3.28	>0.97	0.19	>0.95	389	>0.99	37	>0.99	0.008	0.005
Rh-AMNP	750	2	>0.97	0.10	>0.97	354	>0.99	23	>0.99	0.005	0.004
AMI-25	300	1.98	>0.95	0.57	>0.95	148	>0.95	72	>0.95	0.001	0.008
AMI-25	500	1.02	>0.97	0.22	>0.97	140	>0.97	60	>0.90	0.007	0.004
AMI-25	750	0.79	>0.97	0.15	>0.92	150	>0.97	19	>0.97	0.005	0.008
VSOP C-200	300	4.09	>0.97	0.25	>0.90	79	>0.90	32	>0.90	0.051	0.008
VSOP C-200	500	1.77	>0.97	0.06	>0.97	103	>0.97	30	>0.97	0.017	0.002
VSOP C-200	750	1.57	>0.97	0.14	>0.97	112	>0.97	15	>0.97	0.014	0.009

The values are compared with values for AMNPs obtained from Ref. 9.

Rh-AMNP compartmentalized in cells showed a 17- to 23-fold reduction in molar r_1 relaxivities (r_1: 0.21 [7 T]; 0.19 [11.7 T]; and 0.1 [17.6 T] [mM^{-1} s^{-1}]; Table 2). As in solution, r_1 decreased according to the applied field strength. There was a 7- to 15-fold reduction in r_2 (r_2: 56 [7 T]; 37 [11.7 T]; and 23 [17.6 T] [mM^{-1} s^{-1}]; Table 2) when compared with the free contrast agent. Furthermore, r_2 showed a trend of decreasing values with increasing field strength (Fig. 7). As a result, r_1/r_2 remained mostly unchanged (Table 2).

Comparison of Rh-AMNPs with AMI-25 and VSOP-C200

After cell labeling with AMI-25 and VSOP-C200, a Trypan blue test revealed a high degree of cellular viability. As determined by ICP-MS, the amount of iron was 0.16 ± 0.02 pg per cell (range: 0.14–0.19 pg per cell) after incubation with 100 μg mL^{-1} AMI-25 for 4 h. After labeling with VSOP-C200, the amount of iron was determined to be 1.56 ± 0.21 pg per cell (range: 1.28–1.89 pg per cell; Table 1).

Relaxometry of free AMI-25 at 300, 500, and 750 MHz revealed a longitudinal relaxivity r_1 of 1.98, 1.02, and 0.79 (mM^{-1} s^{-1}) and a transversal relaxivity r_2 of 148, 140, and 150 (mM^{-1} s^{-1}). The resulting r_1/r_2 ranged from 0.013 (7 T) to 0.005 (17.6 T). In contrast, VSOP-C200 showed higher r_1 (4.09, 1.77, 1.57 [mM^{-1} s^{-1}]) and lower r_2 (79, 103, 112 [mM^{-1} s^{-1}]), resulting in an r_1/r_2 ratio of 0.051 (7 T) to 0.012 (17.6 T) (Table 2). The reduction of r_1 and r_2 after cellular internalization was 2- to 8-fold for AMI-25 and 2- to 30-fold for VSOP-C200 (Table 2).

DISCUSSION

Our investigations resulted in three major findings: (a) r_1 and r_1/r_2 of Rh-AMNPs decreases from 7 to 17.6 T while r_2 remains relatively constant above 7 T; (b) cellular internalization decreased the molar relaxivities of Rh-AMNPs 2- to 30-fold at field strengths from 7 T to 17.6 T; and (c) at 17.6 T, these effects were similar for the three different types of SPIOs used in this study.

Relaxivities of Suspended Iron Oxides

Commonly extrapolated NMRD profiles are used to estimate the relaxivities of iron oxide contrast agents at high field strengths. Experimental data on iron oxides above 7 T is lacking. In this study, we found a plateau of r_2 and a decrease of r_1 between 7 T and 17.6 T. This is in line with the observations of others and the estimations obtained from nuclear magnetic relaxation dispersion (NMRD) profiles.

The molar relaxivities of iron oxide nanoparticles often depend on the size and composition of their iron oxide

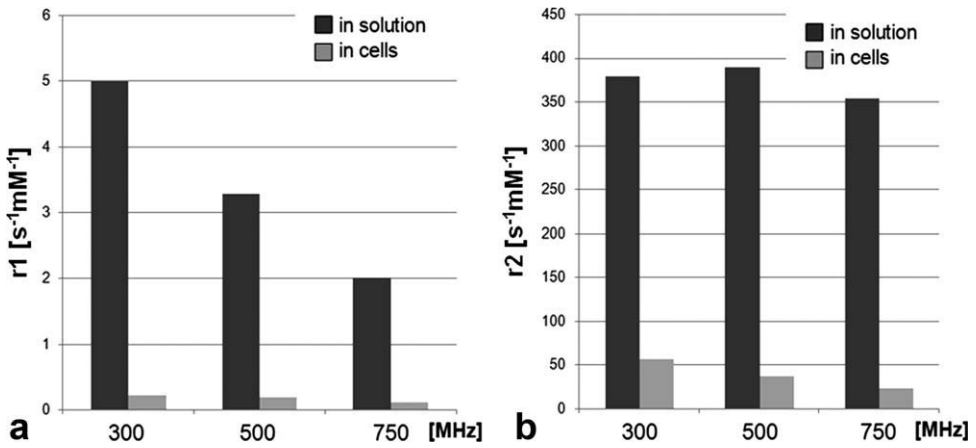

FIG. 7. Comparison of intracellular and extracellular r_1 (**a**) and r_2 (**b**) relaxivities of Rh-AMNPs at different field strengths.

core (16). Both r_1 and r_2 increase with the size of the Fe_3O_4/Fe_2O_3 core; however, r_1/r_2 decreases due to the stronger increase in r_2. This fact might explain the higher T_2 relaxivities of AMNPs observed by us and others (9) when compared with that of VSOPs or SPIOs reported elsewhere (3,10). As shown in Table 2, our results on r_1 and r_2 are consistent with the values reported by Billotey et al. (9) at lower field strengths. Furthermore, the size and composition of the coating material has been shown to significantly influence the T_1 and T_2 behavior of SPIOs (16). This is discussed below in detail.

Finally, the diffusion coefficients of the media used to dilute the contrast agent impacts their "apparent" relaxivities (5). This fact may be accountable for differences in the relaxivities obtained in our study when compared with measurements performed in pure water. To be able to provide constant results on free and internalized contrast agents, we chose to perform all our experiments in Ficoll solution.

Relaxivities of Intracellular Iron Oxides

Importantly, no clusters of cells or local differences in signal intensities due to inhomogeneous distribution of cells in Ficoll solution were observed within a 30-min MR-measurement time. Rather than using histological evaluation to exclude local differences in cell distribution, we preferred the use of susceptibility-sensitive gradient echo sequences with a long TE of 6 ms. Preparation of histological samples (smear slides) can potentially disperse cell clusters in Ficoll solution. Thus, clusters that can be detected with MR measurements might be undetectable in histology.

Previous studies at lower field strengths have covered the topic of changes in the relaxation behavior of SPIOs after cellular internalization (10,17). These observed differences impact not only the choice of pulse sequences and imaging parameters in cell-tracking studies but also the quantification of contrast agent uptake via in vitro or in vivo relaxometry depends on knowledge of changes in relaxivities after cellular uptake (18). While Simon et al. (10) showed a decreased difference for r_1 between 1.5 T (−79%) and 3 T (−48%), and a constant 2- to 3-fold reduction in r_2, Brisset et al. (4) observed increasing differences between 4.7 T (r_1: −62%; r_2: −33%) and 7 T (r_1: −69%; r_2: −55%).

Measurements on intracellular relaxivities are more prone to changes in the experimental setup when compared with relaxometry on freely dispersed iron oxides. An extended number of parameters must be considered, such as the absolute number of cells, the amount of intracellular iron, and the volume fraction of the contrast agent in proportion to the surrounding medium. Our results suggest a pronounced r_2 reduction after cellular internalization at field strengths above 7 T and a constant r_1 reduction for Rh-AMNPs measured above 7 T. These results extend the observations made by Brisset et al. beyond 7 T.

Comparison of Relaxivities: Internalized Versus Suspended

In the experiments, a decrease of r_1 was observed for suspended and internalized contrast agents by increasing field strength. This is in line with the behavior explained by the outer sphere relaxation theory (19,20). As previously stated, the decrease of r_1 with internalization has also been observed and previously described. This is explained by multicompartment exchange models (4,9). Because of the internalization of the nanoparticles into endosomes, an intraendosomal compartment with large r_1 but small volume fraction and another extraendosomal compartment with large volume fraction but small r_1 are present. Although water protons are exchanged between these compartments, the effects of intraendosomal compartmentalization manifest in a reduced "apparent" r_1 of the entire system. However, the overall relaxation time also decreases by increasing field strength because of the significant decrease of the relaxation time of the inner compartment containing the contrast agent at the fields strengths investigated in this work.

In our experiments, the behavior of r_2 with increasing field strength was different for the internalized contrast agent when compared with noninternalized. While the r_2 of the free contrast agent shows a plateau, the internalized contrast agent exhibits a significant decrease of r_2 with increasing field strength. A possible explanation is that at the fields strengths investigated in this work, two different processes with different behaviors contribute to r_2. The first is the quantum mechanical contribution described by outer sphere relaxation theory (6,19–21). The second is the classical incoherent spin dephasing while diffusing in an inhomogeneous magnetic field (22–24).

The second effect has been thoroughly theoretically (22–26) and experimentally (9,11) investigated. The incoherent spin dephasing depends on the size of the particle and the susceptibility difference between the nanoparticle and the surrounding water. For the field strengths investigated in this work (7 T up to 17.6 T), the magnetization of the superparamagnetic particles is saturated and the susceptibility difference does not alter significantly. Thus, one assumes that the part of r_2 arising from incoherent spin dephasing should exhibit no dependence on the field strength of the external field. Incoherent spin dephasing, however, shows a significant dependence on the particle size.

The correlation time of the spin diffusion process inside such field inhomogeneities is given by $\tau = R^2/D$, where R is the typical size of the object creating the field inhomogeneity and D is the diffusion coefficient (27). To efficiently refocus the spins in this case and thus suppress the incoherent spin dephasing, the echo time of the spin echo must be shorter than the correlation time (22,28). For suspended contrast agents, the correlation time ranges from nanoseconds to microseconds. Thus, with normal imaging sequences, the incoherent spin dephasing is unsuppressed and significantly contributes to r_2.

However, if the contrast agent is internalized, the iron oxide nanoparticles concentrate in the cells, forming a large object the size of an endosome or even an entire cell. These objects are in the micrometer range with correspondingly large field inhomogeneities. Thus, the correlation time of the diffusion around these objects (cell or endosome) ranges from microseconds to milliseconds. For such correlation times, incoherent spin dephasing is suppressed using multispin echo sequences (22,28–30).

Thus, at all field strengths, a significant drop in r_2 occurs if the nanoparticles are internalized in cells.

The quantum mechanical contribution described by outer sphere theory shows a similar behavior due to internalization of the contrast agent in cells. This effect is analogous to r_1 (4,9) and should lead to a drop in r_2 if the contrast agent is internalized. The dependence on the field strength, however, is different when compared with that of incoherent spin dephasing. Analogous to r_1, a decrease in r_2 with increasing field strength is theoretically predicted (6,19–21). In contrast to r_1, however, r_2 decreases to a nonvanishing value in the high field limit.

Taking both contributions for the relaxation rate r_2 into account might explain the different behavior for internalized and free iron oxide nanoparticles. For free iron oxide nanoparticles, the experiments show a plateau in r_2 and no significant dependence on the field strength. This implies that, in this case, incoherent spin dephasing dominates the r_2 relaxivity.

For internalized iron oxide nanoparticles, the experiments show a significant drop of r_2 at all field strengths when compared with the suspended contrast agent. This is in agreement with both mechanisms, the incoherent spin dephasing and the outer sphere relaxation theory when it is combined with multicompartment exchange models. The observable decrease of r_2 with increasing field strength, however, may indicate that incoherent spin dephasing (9,11,23,24) is suppressed to an extent where the effects leading to a field strength dependence of the r_2 relaxation (6,19–21) could be observed.

It should be noted that the decrease in r_2 with increasing field strength observed in our study is stronger than that expected from theory. A quantitative description, however, of this effect is difficult as, to the best of the authors' knowledge, a single theoretical model that includes both contributions for contrast agents internalized in cells is unavailable. Thus, further investigation must be performed to fully understand this behavior.

It would be of interest to investigate the dependence of the r_1/r_2 ratio on different field strengths for suspended and internalized contrast agents. While in the suspended case the ratio decreases with increasing field strength, it remains relatively constant when the contrast agent is internalized. This is surprising as this effect is neither predicted by outer sphere theory nor by the incoherent spin dephasing. However, as the r_1/r_2 ratio is very low at these field strengths (cf. Table 1), the r_1 effect of the investigated internalized contrast agent might be of no practical interest. Nevertheless, this behavior is interesting from a theoretical point of view and thus should be further investigated.

The determination of r_2* was beyond the scope of this study. This is mainly due to technical difficulties when trying to quantify T_2* on high-field systems. The homogeneity of the main magnetic field becomes critically necessary at field strengths up to 17.6 T. So far, we cannot guarantee sufficient field homogeneity for all three field strengths used in this study.

Comparison of Rh-AMNPs with AMI-25 and VSOP-C200

As previously shown, size (31,32) and surface charge are major determinants of the cellular uptake of iron oxides (33). Although we used a standardized label protocol for all contrast agents, the iron content (picogram per cell) showed variations between the different types of contrast agents. Remarkably, smaller iron oxides (AMNP, VSOP) showed higher uptake, which is most likely due to their anionic surface coating (32–34).

The variation of intracellular iron concentrations might hamper comparability between the three contrast agents. Importantly, regarding Rh-AMNPs, we investigated the impact of constant iron content (picogram per cell) and varying amounts of cells. The impact of the opposite situation (constant numbers of cells, varying pg Fe per cell) on r_1 and r_2 relaxivities was not within the scope of this study.

We believe that our experiments more accurately represent the in vivo situation or cell transplantation studies as a defined mean iron concentration per cell would likely be achieved in these scenarios. Kuhlpeter et al. (18) stated that only the total internalized iron amount per volume influences r_2/r_2*. Bowen et al., however, demonstrated a difference in the R_2 relaxation rates for a constant total internalized iron amount. The difference is dependent on whether the cell number is varied or the iron load of the cells (11). This issue has not been covered in our work and should be investigated in further studies.

The different coating materials, hydrodynamic diameters, and iron cores must also be accounted for as they predominately impact the relaxation properties of SPIOs. Differences in iron core diameters might further explain the less pronounced decrease in r_2 of commercially available AMI-25 and VSOPs when compared with Rh-AMNPs. The 2- to 30-fold reduction of the molar relaxivities of three iron oxide contrast agents at 17.6 T, however, allows us to conclude that internalization of iron oxides leads to a distinct decrease in r_1 and r_2 at very high field strengths.

Limitations

Although the volume fractions of cells seem low in our experimental setup (0.17% to 1.32% by volume), the absolute numbers and volumes used in this study seem appropriate with respect to possible in vivo conditions (e.g., in vivo labeled macrophages) or cell transplantation experiments (10). Nevertheless, results may significantly vary when performed with different volume fractions of cells.

Finally, we recognize that the iron loading levels of 0.16–1.47 pg Fe per cell are lower than those typically found with similar nanoparticles and similar phagocytic cell lines (35). Higher levels may be achieved by varying the iron oxide concentration (36) or incubation times. The r_1 and r_2 findings in this article must be understood in this context. Furthermore, the principal finding of strongly decreased r_1 and r_2 on cellular compartmentalization at very high field may vary with higher cellular iron oxide loading levels.

CONCLUSIONS

Expanding on previous experiments, we have shown that r_1 and r_2 relaxivities of intracellular iron oxides

strongly decrease with cellular internalization. These results should be considered while performing T_1- or T_2-weighted imaging with T_2* insensitive sequences at very high field strengths. Further studies should address the topic of r_2* and the different ratios of iron per cell for optimizing cellular imaging parameters at fields above 7 T.

ACKNOWLEDGMENTS

The authors thank Martina Regensburger for cell labeling, and Christian Stötzel for performing ICP-MS analysis. Histochemistry and immunohistochemistry were performed by Elisabeth Bauer. TEM imaging was performed in the Fraunhofer-Institut für Silicatforschung by A.K. Löbmann. Christian H. Ziener thanks the Berufsverband Deutscher Internisten for providing a scholarship. We thank the Deutsche Forschungsgemeinschaft for funding (DFG-SFB 688).

REFERENCES

1. Clarke SE, Weinmann HJ, Dai E, Lucas AR, Rutt BK. Comparison of two blood pool contrast agents for 0.5-T MR angiography: experimental study in rabbits. Radiology 2000;214:787–794.
2. Wunderbaldinger P, Josephson L, Weissleder R. Crosslinked iron oxides (CLIO): a new platform for the development of targeted MR contrast agents. Acad Radiol 2002;9 (Suppl 2):S304–S306.
3. Taupitz M, Wagner S, Schnorr J, Kravec I, Pilgrimm H, Bergmann-Fritsch H, Hamm B. Phase I clinical evaluation of citrate-coated monocrystalline very small superparamagnetic iron oxide particles as a new contrast medium for magnetic resonance imaging. Invest Radiol 2004;39:394–405.
4. Brisset JC, Desestret V, Marcellino S, Devillard E, Lagrade F, Nighoghossian N, Berthezene Y, Wiart M. T1 and T2 quantification of free USPIO and USPIO-labeled macrophages at 4.7T and 7T. Proc Int Soc Mag Res Med 2008;16:1687.
5. Bulte JW, Vymazal J, Brooks RA, Pierpaoli C, Frank JA. Frequency dependence of MR relaxation times. II. Iron oxides. J Magn Reson Imaging 1993;3:641–648.
6. Corot C, Robert P, Idee JM, Port M. Recent advances in iron oxide nanocrystal technology for medical imaging. Adv Drug Deliv Rev 2006;58:1471–1504.
7. Nahrendorf M, Jaffer FA, Kelly KA, Sosnovik DE, Aikawa E, Libby P, Weissleder R. Noninvasive vascular cell adhesion molecule-1 imaging identifies inflammatory activation of cells in atherosclerosis. Circulation 2006;114:1504–1511.
8. Bertorelle F, Wilhelm C, Roger J, Gazeau F, Menager C, Cabuil V. Fluorescence-modified superparamagnetic nanoparticles: intracellular uptake and use in cellular imaging. Langmuir 2006;22:5385–5391.
9. Billotey C, Wilhelm C, Devaud M, Bacri JC, Bittoun J, Gazeau F. Cell internalization of anionic maghemite nanoparticles: quantitative effect on magnetic resonance imaging. Magn Reson Med 2003;49:646–654.
10. Simon GH, Bauer J, Saborovski O, Fu Y, Corot C, Wendland MF, Daldrup-Link HE. T1 and T2 relaxivity of intracellular and extracellular USPIO at 1.5T and 3T clinical MR scanning. Eur Radiol 2006; 16:738–745.
11. Bowen CV, Zhang X, Saab G, Gareau PJ, Rutt BK. Application of the static dephasing regime theory to superparamagnetic iron oxide loaded cells. Magn Reson Med 2002;48:52–61.
12. Sun S, Zeng H, Robinson DB, Raoux S, Rice PM, Wang SX, Li G. Monodisperse MFe_2O_4 (M = Fe, Co, Mn) nanoparticles. J Am Chem Soc 2004;126:273–279.
13. Kohler N, Fryxell GE, Zhang M. A bifunctional poly(ethylene glycol) silane immobilized on metallic oxide-based nanoparticles for conjugation with cell targeting agents. J Am Chem Soc 2004;126:7206–7211.
14. Adami C, Brunda MJ, Palleroni AV. In vivo immortalization of murine peritoneal macrophages: a new rapid and efficient method for obtaining macrophage cell lines. J Leukoc Biol 1993;53:475–478.
15. Deichmann R, Haase A. Quantification of Tl values by SNAPSHOT-FLASH NMR imaging. J Magn Reson 1992;96:608–612.
16. LaConte LE, Nitin N, Zurkiya O, Caruntu D, O'Connor CJ, Hu X, Bao G. Coating thickness of magnetic iron oxide nanoparticles affects R2 relaxivity. J Magn Reson Imaging 2007;26:1634–1641.
17. Billotey C, Aspord C, Beuf O, Piaggio E, Gazeau F, Janier MF, Thivolet C. T-cell homing to the pancreas in autoimmune mouse models of diabetes: in vivo MR imaging. Radiology 2005;236:579–587.
18. Kuhlpeter R, Dahnke H, Matuszewski L, Persigehl T, von Wallbrunn A, Allkemper T, Heindel WL, Schaeffter T, Bremer C. R2 and R2* mapping for sensing cell-bound superparamagnetic nanoparticles: in vitro and murine in vivo testing. Radiology 2007;245:449–457.
19. Koenig SH, Kellar KE. Theory of 1/T1 and 1/T2 NMRD profiles of solutions of magnetic nanoparticles. Magn Reson Med 1995;34: 227–233.
20. Laurent S, Forge D, Port M, Roch A, Robic C, Vander Elst LV, Muller RN. Magnetic iron oxide nanoparticles: synthesis, stabilization, vectorization, physicochemical characterizations, and biological applications. Chem Rev 2008;108:2064–2110.
21. Roch A, Muller RN, Gillis P. Theory of proton relaxation induced by superparamagnetic particles. J Chem Phys 1999;110:5403–5411.
22. Jensen JH, Chandra R. NMR relaxation in tissues with weak magnetic inhomogeneities. Magn Reson Med 2000;44:144–156.
23. Ziener CH, Bauer WR, Jakob PM. Transverse relaxation of cells labeled with magnetic nanoparticles. Magn Reson Med 2005;54: 702–706.
24. Jensen JH, Chandra R. Strong field behavior of the NMR signal from magnetically heterogeneous tissues. Magn Reson Med 2000;43: 226–236.
25. Brown RJS. Distribution of fields from randomly placed dipoles: free-precession signal decay as result of magnetic grains. Phys Rev 1961; 121:1379–1382.
26. Yablonskiy DA, Haacke EM. Theory of NMR signal behavior in magnetically inhomogeneous tissues: the static dephasing regime. Magn Reson Med 1994;32:749–763.
27. Ziener CH, Bauer WR, Melkus G, Weber T, Herold V, Jakob PM. Structure-specific magnetic field inhomogeneities and ist effect on the correlation time. Magn Reson Imaging 2006;24:1341–1347.
28. Ziener CH, Kampf T, Jakob PM, Bauer WR. Diffusion effects on the CPMG relaxation rate in a dipolar field. J Magn Reson 2010;202: 38–42.
29. Carr HY, Purcell EM. Effects of diffusion on free precession in nuclear magnetic resonance experiments. Phys Rev 1954;94:630–638.
30. Gillis P, Koenig SH. Transverse relaxation of solvent protons induced by magnetized spheres: application to ferritin, erythrozytes, and magnetite. Magn Reson Med 1987;5:323–345.
31. Bulte JW, Zhang S, van Gelderen P, Herynek V, Jordan EK, Duncan ID, Frank JA. Neurotransplantation of magnetically labeled oligodendrocyte progenitors: magnetic resonance tracking of cell migration and myelination. Proc Natl Acad Sci USA 1999;96:15256–15261.
32. Metz S, Bonaterra G, Rudelius M, Settles M, Rummeny EJ, Daldrup-Link HE. Capacity of human monocytes to phagocytose approved iron oxide MR contrast agents in vitro. Eur Radiol 2004;14: 1851–1858.
33. Wilhelm C, Billotey C, Roger J, Pons JN, Bacri JC, Gazeau F. Intracellular uptake of anionic superparamagnetic nanoparticles as a function of their surface coating. Biomaterials 2003;24:1001–1011.
34. Fleige G, Seeberger F, Laux D, Kresse M, Taupitz M, Pilgrimm H, Zimmer C. In vitro characterization of two different ultrasmall iron oxide particles for magnetic resonance cell tracking. Invest Radiol 2002;37:482–488.
35. Corot C, Port M, Guilbert I, Robert P, Raynal I, Robic C, Raynaud J-S, Prigent P, Dencausse A, Idee J-M. Superparamagnetic contrast agents. In: Modo MMJ, Jeff WM, Bulte JWM, editors. Molecular and cellular MR imaging. CRC Press; Boca Raton, FL. 2007. p. 59–84.
36. Klug G, Bremicker J, Kampf T, Bauer E, Basse-Lüsebrink T, Weber M, Gbureck U, Nöth U, Jakob PM, Bauer WR. Detection limits of very small iron oxide nanoparticles in labeled cells: a quantitative evaluation of histochemistry and MR-relaxometry. Proc Int Soc Mag Res Med 2009;17:906.